JMEPEG (2010) 19:1214–1219
DOI: 10.1007/s11665-010-9603-7

1059-9495/$19.00

Temperature Dependence of Tensile Behaviors of Nitrogen-Alloyed Austenitic Stainless Steels

Wei Wang, Wei Yan, Ke Yang, Yiyin Shan, and Zhouhua Jiang

(Submitted June 14, 2009; in revised form December 6, 2009)

The temperature dependence of tensile behaviors of two nitrogen-alloyed austenitic stainless steels, an annealed 316LN steel and a high-nitrogen austenitic stainless steel (Fe-Cr-Mn-0.66% N), was investigated by tensile test at different temperatures from 293 K down to 77 K. It was found that strength of the two steels increased with decrease of temperature. With a decrease in temperature, the uniform elongation increased for the 316LN steel, whereas it increased followed by a decrease for the high-nitrogen steel. A three-stage hardening behavior occurred in the 316LN steel, but not in the high-nitrogen steel, with decrease of temperature. The strain-induced martensite transformation in the 316LN steel could retard void nucleation and increase the strain-hardening rate, resulting in much higher tensile stress and higher uniform elongation of 316LN steel. It was analyzed that stacking fault energy of the high-nitrogen steel decreased with decrease of temperature, which promoted the twinning and planar slipping in the steel, and resulted in brittle fracture at cryogenic temperatures.

Keywords high-nitrogen stainless steel, stacking fault energy, strain-hardening rate, strain-induced martensite, tensile properties

1. Introduction

Nitrogen-alloyed austenitic stainless steels possess high resistance to corrosion, and have good work-hardening ability, high strength, and excellent ductility over a wide temperature range (Ref 1-4). Furthermore, nitrogen-alloyed austenitic stainless steels have more stable austenitic structures due to the strong austenite-stabilizing ability of nitrogen. No phase transformation occurred in high-nitrogen austenitic stainless steels even at cryogenic temperature or after severe cold deformation (Ref 5). Owing to the above beneficial effects and the progress on nitrogen steel processing technologies, nitrogen addition in steels has received increased attention.

However, nitrogen alloying may also cause some negative effects. For example, the ductile-to-brittle transition phenomenon in the nitrogen-alloyed steels relates to unusual cleavage-like fractures at cryogenic temperatures, even though these steels have f.c.c. structures (Ref 6-11). To better understand the brittle fracture mechanism for high-nitrogen steels, it is necessary to further study the mechanical properties, stress-strain behaviors, and microstructures of these steels at different temperatures. Several models have been proposed to clarify the deformation behaviors and fracture mechanisms of high-nitrogen steels. Wu et al. (Ref 12) found that the stacking fault energy (SFE) of 316L stainless steel increased, the flow localization occurred, and the mechanical twinning disappeared when the temperature was increased to 493 K. Byun et al. (Ref 13) studied the temperature dependence of strain hardening and plastic instability behaviors in austenitic stainless steels. Their results showed that twins, stacking fault, and martensite laths could be formed at subzero temperatures, and the dislocation-dominant microstructures at elevated temperatures. They believed that the low SFE could not explain the re-acceleration of strain hardening, and the strain (or stress)-assisted martensites provided a less exhaustible hardening mechanism. However, the temperature dependence of stress-strain behaviors of high-nitrogen austenitic stainless steels was not studied systematically.

In this study, a nitrogen-alloyed 316L steel and a high-nitrogen Fe-Cr-Mn austenitic stainless steel were studied for their plastic deformations and fracture behaviors from room temperature down to cryogenic temperature. Observations on the tensile specimens were made under both scanning electron microscopy (SEM) and transmission electron microscopy (TEM). Phase constituents near the fracture surfaces of tensile specimens were measured by x-ray diffraction (XRD).

2. Experimental Procedure

Two steels, 17Cr-12Ni-2Mo-0.1N (named 316LN) and 18Cr-16Mn-2Mo-0.66N (named M66), were used in this investigation. Their chemical compositions are listed in Table 1. The 316LN steel bars were as-received with 20 mm in diameter. The M66 steel was produced by vacuum induction melting and electro-slag remelting. The M66 ingot was hot-forged and hot-rolled into sheets with thickness of 12 mm. These bars and sheets were solution-treated at 1100 °C for 2 h, and then water quenched. All of the materials were confirmed to be of single austenitic phase by XRD analyses and optical microscopy.

Wei Wang, Institute of Metal Research, Chinese Academy of Sciences, Shenyang 110016, P.R. China and Graduate University of Chinese Academy of Sciences, Beijing 100080, P.R. China; **Wei Yan, Ke Yang,** and **Yiyin Shan**, Institute of Metal Research, Chinese Academy of Sciences, Shenyang 110016, P.R. China; and **Zhouhua Jiang**, School of Materials and Metallurgy, Northeastern University, Shenyang 110014, P.R. China. Contact e-mails: wangw@imr.ac.cn and kyang@imr.ac.cn.

Tensile specimens, with gage section dimensions of 30 mm in length and 5 mm in diameter, were cut from the solution-treated 316LN bars along the longitude direction, and the solution-treated M66 sheets parallel to the rolling direction. Tensile tests were performed in the temperature range of 77 to 293 K with a nominal strain rate of 5.6×10^{-4} s^{-1}. The true stress-strain rates were calculated from the load-displacement measurements.

Fracture surfaces were observed on SEM. For TEM observations, thin foils were carefully prepared from fractured specimens of tensile specimens in such a way that foil planes were parallel and close to the fractured surfaces. Disks cut from the specimens were finally electropolished using twin-jet method. TEM observations were conducted using a TEM of Phillips TECNAI20 operated at 120 kV. XRD measurement was carried out near the fracture surface of the specimens after tensile testing at 77 K.

After tensile failure, the neck diameter of specimens was measured using a micrometer to obtain the final cross-sectional area A_F. True fracture strain, ε_F, and true fracture stress, σ_F, were calculated from the initial and final cross-sectional area A_0 and A_F, respectively, as well as the fracture load P_F by the following relationships (Ref 13):

$$\varepsilon_F = \ln(A_0/A_F) \qquad \text{(Eq 1)}$$

$$\sigma_F = P_F/A_F \qquad \text{(Eq 2)}$$

3. Experimental Results

3.1 Strain-Hardening Behaviors

Figure 1 presents the true stress-strain curves and the instantaneous strain-hardening rate ($n_T = d\sigma/d\varepsilon$)-strain curves of the two nitrogen-alloyed austenitic stainless steels at the selected temperatures. The intersection point of the two curves corresponds to the onset of necking. These steels showed strong temperature dependences of both strength and plasticity.

It can be seen in Fig. 1(a) that the plasticity of the 316LN steel increased with decrease of temperature down to 77 K, showing high uniform elongation of 40 to 50% above 77 K. Except for 77 K, the true stress of the 316LN steel increased linearly with the true strain until fracture. At 77 K, however, the true stress-strain curve showed three-stage hardening behavior. As shown in Fig. 1(b), the strength of the M66 steel increased with decrease of temperature, but the uniform elongation increased with temperature from 293 to 213 K, and then began to decrease with further decrease of temperature. It was also found that, except for the specimen tested at 77 K, all the tensile specimens of the steel showed high uniform elongations of 40 to 50% and relatively small necking elongation. However, the fracture occurred without necking for the steel after a small strain at 77 K, resulting in a very small uniform elongation.

The strain-hardening rate of both the experimental steels at different temperatures decreased monotonically with strain in the uniform deformation region. Much higher n_T was found at the onset of deformation, but it rapidly decreased with strain in the true strain range of 0 to 0.05. This rapid decrease of strain-hardening rate had been explained by dislocation multiplication prior to large-scale plastic deformation (Ref 12). For the 316LN steel at 213 K and above, the rapid decreasing stage of the strain-hardening rate was followed by a linear decreasing stage, where the strain-hardening rate decreased linearly with increase of true strain, and another rapid decreasing stage occurred as the strain approached the intersection point, i.e., the onset point of necking. However, when temperature was further decreased to 173 K, the curve of strain-hardening rate versus true strain became concave upward in the uniform deformation region. At 133 K and below, the strain-hardening curves showed a three-stage hardening behavior, which comprised a rapid decreasing stage (stage A) and an acceleration hardening stage (stage B) and then a rapid decreasing stage again (stage C). The true strain in the decrease-increase inflexion region was decreased with decrease of temperature, about 0.22 and 0.11 at 133 and 77 K, respectively. The strain-hardening rate in the inflexion was also decreased with decrease of temperature, about 1770 and 1400 MPa at 133 and 77 K, respectively. After the decrease-increase inflexion, the strain-hardening rate

Table 1 Chemical composition of the experimental steels

Steel name	N	Cr	Ni	Mn	Mo	C	Si	S	P
	Composition, wt.%								
316LN	0.14	15.30	12.54	1.48	2.50	0.01	0.21	0.0030	0.008
M66	0.66	18.36	···	15.81	2.19	0.04	0.24	0.0038	0.017

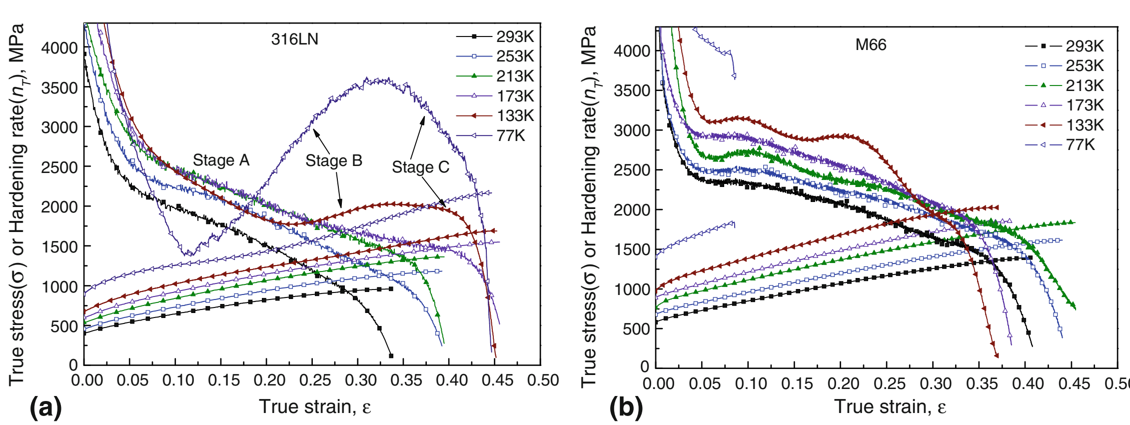

Fig. 1 Temperature dependence of true stress-true strain curves of 316LN (a) and M66 (b) steels

increased with further deformation, and the increasing rate was increased with decrease of temperature. The strain-hardening rate curve had a maximum in stage B, which was increased with decrease of temperature, about 2020 and 3600 MPa at 133 and 77 K, respectively, at a true strain of about 0.32. Byun et al. (Ref 13) studied the strain-stress behaviors of a kind of 316LN steel and obtained results consistent with this work. Due to the acceleration of strain hardening in stage B, the true stress increased rapidly and the necking occurred at fairly high strain level.

For the M66 steel at all the testing temperatures, no stage B could be found in the strain-hardening rate versus true strain curves. The uniform elongation increased with decrease of temperature from 293 to 213 K, and then began to decrease with further decrease of temperature. In general, the n_T-strain curve displays a two-stage hardening behavior at low temperature for a stainless steel, but the M66 steel in this work did not show such a tendency at the selected temperature. At 133 K, the n_T fluctuated within a narrow range, and then decreased rapidly with increase of the true strain, which did not lead to a beginning of the necking. When the testing temperature was 77 K, the n_T dropped rapidly from 4000 MPa and a no-necking brittle fracture occurred, which indicated that the cracking was initiated and grew fast after the deformation.

3.2 Fractography of the Tensile Fracture

Figure 2 shows the typical SEM fracture morphologies of the 316LN steel (Fig. 2a, b) and the M66 steel (Fig. 2c, d) obtained from observations on tensile fractured surfaces tested at 293 and 77 K, respectively. The fracture surface of the 316LN steel was completely ductile and the entire surface consisted of dimples. Compared to Fig. 2(b), deeper and larger dimples can be seen in Fig. 2(a). It can be concluded that voids would grow more easily at 77 K than that at 293 K in the steel, and the necking strain, i.e., the difference between uniform and total elongations, at 77 K would be much smaller than that at 293 K.

The fracture morphology of the M66 steel at 293 K was similar to that of the 316LN steel, as shown in Fig. 2(c), which indicates severe deformation in this region and wide-spread deformation throughout the specimen. However, when temperature was decreased to 77 K, a cleavage-like fracture occurred in the M66 steel and the fracture surface consisted of flat facets surrounded by tear edges, as shown in Fig. 2(d). This kind of fracture surface was also observed on the impact brittle surface at subzero temperature (Ref 6, 7, 9-11), and the flat facets always contained very straight slip lines. These flat facets were determined as (111) planes as reported by Tobler and Meyn (Ref 6). These straight slip lines on (111) planes were considered as the crack sources, obeying the slipping-off mechanism also based on the results (Ref 10).

3.3 Temperature Dependence of Microstructures

Figure 3 shows the XRD results obtained near the tensile fractured surface of the two steels at 77 K. Diffraction peaks of the α′ martensite are evident in the 316LN steel at 77 K, and the retained austenite in the specimen was only negligible. For the M66 steel at 77 K, however, only the austenite diffraction peak appeared as shown in Fig. 3. In general, the austenite structures in the two steels should be thermodynamically stable in the testing temperature range. Therefore, the α′ martensite found in the 316LN steel should be strain-induced. The ε martensite diffraction peak was not detected in the two steels. Byun et al. (Ref 13) also observed lots of α′ martensites

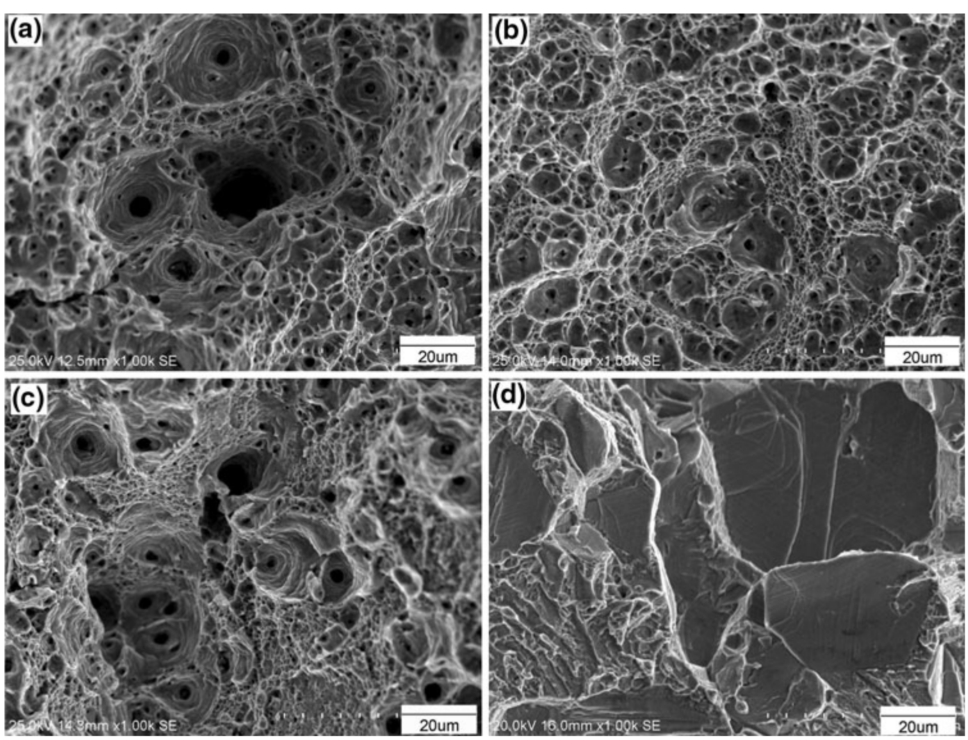

Fig. 2 Typical SEM fractographies of the tensile fractured surfaces at 293 K (a) and (c), 77 K (b) and (d) for 316LN (a, b) and M66 (c, d) steels

in the uniform elongation section of a 316LN steel after 50% tensile deformation at 123 K by TEM. When temperature was increased to 473 K, no martensite was observed, and the strain-hardening behavior was same to that of the M66 steel.

Figure 4 shows the TEM observations on the M66 steel tensile tested at 133 K. Dense, tangled dislocations, seen as dark patches, became abundant, but the dislocation density among the slip bands was very low. It can also be seen from Fig. 4(b) that the intensive interactions among the slip bands have caused serious torsions at intersections of the slip bands, as indicated by the white arrows. TEM observation on the specimen tested at 77 K was also made as shown in Fig. 5(a), in which the microstructures after deformation consisted of tangled dislocations and high-density stacking faults.

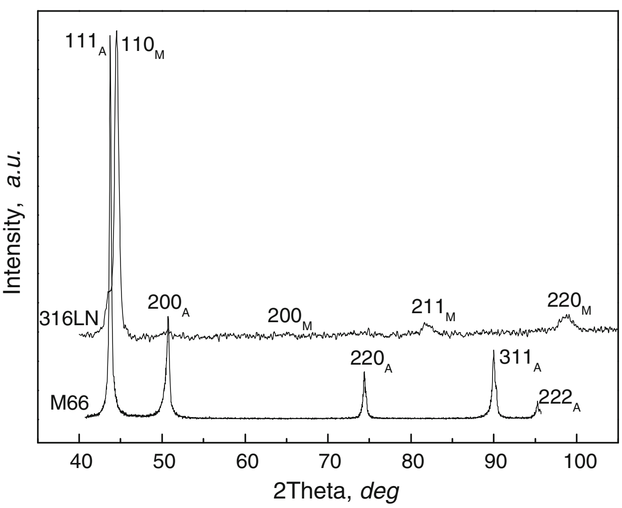

Fig. 3 X-ray diffractograms near the tensile fractured surface of 316LN and M66 tested at 77 K

4. Discussion

In general, strain can assist the martensitic transformation in austenitic steels. The transformation produces about 20% shear strain as well as a volume expansion with maximum of about 5% (Ref 14, 15). Therefore, at the initial stage (corresponding to stage A) of martensitic transformation, the strain-hardening rate could be decreased due to the volume expansion. When the fraction of martensite is large enough, the steel should be hardened by large number of hard martensites and the strain-hardening rate should be increased rapidly (as stage B). As the stress increases, martensites begin to deform and the strain-hardening rate should decrease with slow transformation of the retained austenite to martensite (the stage C). The strain-induced martensite could retard the void nucleation and increase the strain-hardening rate, and then result in a much high fracture stress and a high uniform elongation in the 316LN steel.

Due to the stable austenite structure, strain-induced martensitic transformation did not occur in the M66 steel. It was confirmed that low SFE and extended dislocations were identified as being of crucial importance with regard to the deformation behavior of austenitic steels (Ref 13, 16, 17). Galvriljuk et al. (Ref 18) reported that nitrogen caused a sharp decrease of the SFE with decrease of temperature, while no marked temperature dependence of the SFE was observed in carbon steels. However, scant work has been reported on this phenomenon in the nickel-free austenitic steels.

To clarify the temperature dependence of SFE for high-nitrogen Fe-Cr-Mn austenitic stainless steel, TEM observation on the M66 steel after 10% cold rolling was made to compare with the steel tensile tested at 77 K with about 10% engineering strain near the tensile fractured surface, as shown in Fig. 5. At 77 K, the deformation microstructure in the steel consisted of tangled dislocations and high-density stacking faults, as shown in Fig. 5(a). However, it can be found in Fig. 5(b) that density of the stacking fault was very low, and no apparent planar

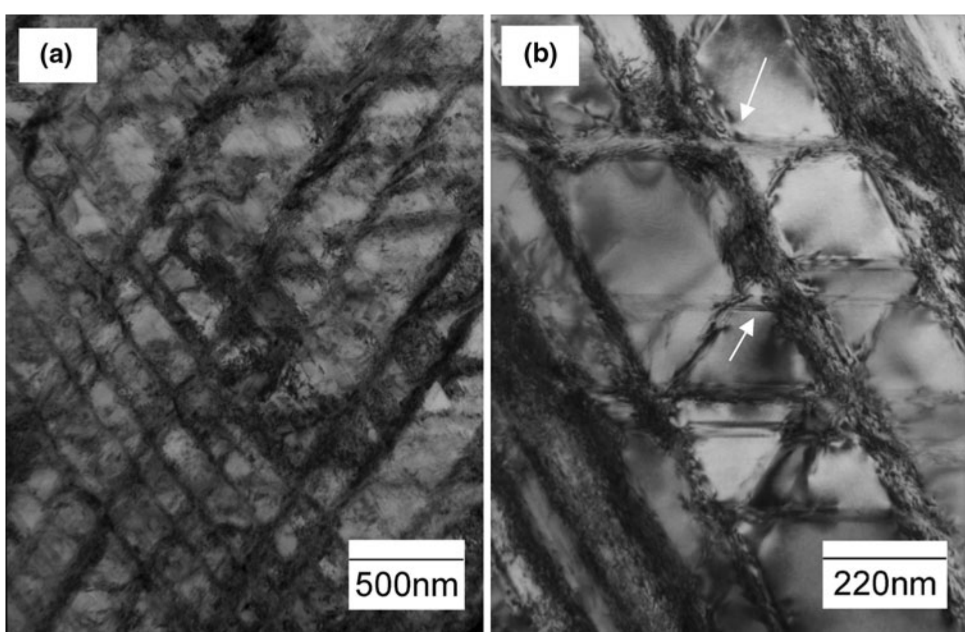

Fig. 4 Planar slipping with high density of dislocations in M66 steel after deformation at 133 K

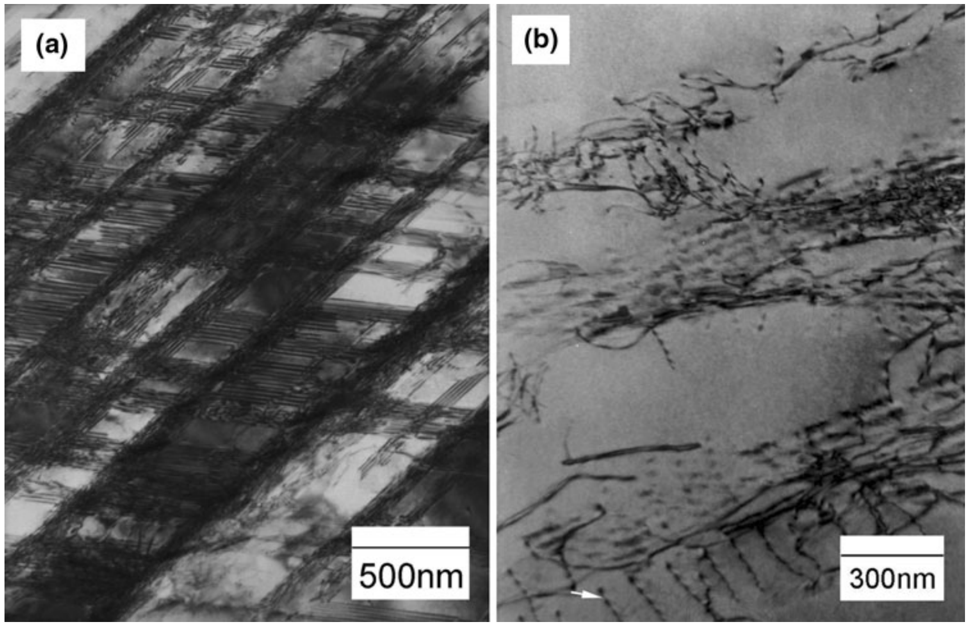

Fig. 5 TEM observations on M66 steel after 10% cold deformation at 77 K (a) and 293 K (b)

dislocation slip was observed. Therefore, it can be concluded that the SFE of the M66 steel should decrease with decrease of temperature.

Figure 4 and 5(a) shows the microstructure change of the deformed M66 steel at 133 and 77 K. At 133 K, planar slipping and tangling of dislocations were the main hardening mechanism, and planar slipping also encouraged annihilation of dislocations by increasing the possibility of intensive interactions among slip bands and serious torsions at the intersection of slip bands. However, at 77 K, the SFE of the steel decreased and high-density stacking faults can be observed. These stacking faults turned out as new obstacles to the later slipping dislocations during deformation, which should produce a higher strain-hardening rate.

Theoretically, high strain-hardening rate makes the plastic deformation from local area spread into a larger volume in material, thus delaying the strain localization or necking, but Fig. 1(b) shows an opposite result. It has been confirmed (Ref 2, 16, 17) that the planar dislocation interaction determines the work-hardening behavior of nitrogen-alloyed austenitic stainless steels, especially at low temperature. Hence, at cryogenic temperature of 77 K, the SFE of the M66 steel can further promote the planar slipping. Tomota et al. (Ref 11) named this fracture mechanism as "slipping-off," which could accelerate the crack nucleation, and then speed the brittle fracture to occur. Based on the above analyses, low ductility of the M66 steel at 77 K should be caused by both the absence of strain-induced martensite, which could reduce the stress concentration and hinder the crack growth as well, and the formation of cracks induced by dislocation slipping.

5. Conclusions

Temperature dependence of tensile behaviors of two nitrogen-alloyed austenitic stainless steels was investigated by tensile test in the temperature range of 77 and 293 K. The following conclusions are drawn from this work:

1. The strength of the two steels increased with decrease of temperature. The uniform elongation increased for the 316LN steel, whereas it increased followed by a decrease for the M66 steel, with decrease of temperature.
2. The fracture surface of the 316LN steel was completely ductile at 293 and 77 K. The fracture morphology of the M66 steel was similar to that of the 316LN steel at 293 K, but cleavage-like fracture occurred and the fracture surface consisted of flat facets surrounded by tear edges at 77 K.
3. The strain-hardening rate of the 316LN steel decreased monotonically with strain in the flow region at 213 K or above, but became concave upward in the uniform deformation region at 173 K, and showed a three-stage hardening behavior when temperature decreased to 133 K or below, i.e., a rapid decreasing stage and an acceleration hardening stage, and then a rapid decreasing stage again. However, there was no acceleration hardening stage for the M66 steel at all the testing temperatures.
4. The α' martensite transformation was detected in the deformed 316LN steel at 77 K; however, the M66 steel kept single austenite at the same temperature. The three-stage hardening behavior and the temperature dependence of the tensile stress could be explained by the strain-induced martensitic transformation. Decrease of SFE of the high-nitrogen austenitic stainless steel with decrease of temperature could promote the twinning and planar slipping, and thus result in brittle fracture at cryogenic temperature.

Acknowledgment

The authors gratefully acknowledge the funding from National Natural Sciences Foundation of China (No. 50534010).

References

1. F.M. Bayoumi and W.A. Ghanem, Effect of Nitrogen on the Corrosion Behavior of Austenitic Stainless Steel in Chloride Solutions, *Mater. Lett.*, 2005, **59**, p 3311–3314
2. J.W. Simmons, Overview: High-Nitrogen Alloying of Stainless Steels, *Mater. Sci. Eng. A*, 1996, **207**, p 159–169
3. H. Baba, T. Kodama, and Y. Katada, Role of Nitrogen on the Corrosion Behavior of Austenitic Stainless Steels, *Corros. Sci.*, 2002, **44**, p 2393–2407
4. E. Werner, Solid Solution and Grain Size Hardening of Nitrogen-Alloyed Austenitic Steels, *Mater. Sci. Eng. A*, 1988, **101**, p 93–98
5. S. Wang, K. Yang, Y. Shan, and L. Li, Study on Cold Deformation Behaviors of a High Nitrogen Austenitic Stainless Steel and 316L Stainless Steel, *Acta Metall. Sin.*, 2007, **43**, p 171–176
6. R.L. Tobler and D. Meyn, Cleavage-Like Fracture Along Slip Planes in Fe-18Cr-3Ni-13Mn-0.37N Austenitic Stainless Steel at Liquid Helium Temperature, *Metall. Trans. A*, 1988, **19**, p 1626–1631
7. Y. Tomota and E. Satoshi, Cleavage-Like Fracture at Low Temperatures in an 18Mn-18Cr-0.5N Austenitic Steel, *ISIJ Int.*, 1990, **30**, p 656–662
8. P. Mullner, C. Solenthaler, P. Uggowitzer, and M.O. Speidel, Brittle Fracture in Austenitic Steel, *Acta Metall. Mater.*, 1994, **42**, p 2211–2217
9. J.B. Vogt, A. Messai, and J. Foct, Cleavage Fracture of Austenite Induced by Nitrogen Supersaturation, *Scripta Metall.*, 1994, **31**, p 549–554
10. Y. Tomota, Y. Xia, and K. Inoue, Mechanism of Low Temperature Brittle Fracture in High Nitrogen Bearing Austenitic Steels, *Acta Mater.*, 1998, **46**, p 1577–1587
11. Y. Tomota, J. Nakano, Y. Xia, and K. Inoue, Unusual Strain Rate Dependence of Low Temperature Fracture Behavior in High-Nitrogen Bearing Austenitic Steels, *Acta Mater.*, 1998, **46**, p 3099–3108
12. X. Wu, X. Pan, J.C. Mabon, M. Li, and J.F. Stubbins, The Role of Deformation Mechanisms in Flow Localization of 316L Stainless Steel, *J. Nucl. Mater.*, 2006, **356**, p 70–77
13. T.S. Byun, N. Hashimoto, and K. Farrell, Temperature Dependence of Strain Hardening and Plastic Instability Behaviors in Austenitic Stainless Steels, *Acta Mater.*, 2004, **52**, p 3889–3899
14. R.H. Leal, "Transformation Toughening of Metastable Austenitic Steels," Ph.D. Thesis, MIT, Cambridge, MA, 1984
15. J.R. Patel and M. Cohen, Criterion for the Action of Applied Stress in the Martensitic Transformation, *Acta Metall.*, 1953, **1**, p 531–538
16. K. Satoru, Y. Xia, and Y. Tomata, Work-Hardening Behavior and Evolution of Dislocation Microstructures in High-Nitrogen Bearing Austenitic Steels, *ISIJ Int.*, 1998, **38**, p 474–481
17. G. Saller, K. Spiradek-Hahn, C. Scheu, and H. Clemens, Microstructural Evolution of Cr-Mn-N Austenitic Steels During Cold Work Hardening, *Mater. Sci. Eng. A*, 2006, **427**, p 246–254
18. V.G. Gavriljuk, A.L. Sozinov, J. Foct, J.N. Petrov, and Y.A. Polushkin, Effect of Nitrogen on the Temperature Dependence of the Yield Strength of Austenitic Steels, *Acta Mater.*, 1998, **46**, p 1157–1163